Journal of Controlled Release 360 (2023) 747–758

Contents lists available at ScienceDirect

Journal of Controlled Release

journal homepage: www.elsevier.com/locate/jconrel

Biofunctionalization of 3D printed collagen with bevacizumab-loaded microparticles targeting pathological angiogenesis

Anna Abbadessa [a,b], Paulina Nuñez Bernal [c], Giorgio Buttitta [a,b,1], Alfredo Ronca [d], Ugo D'Amora [d], Carla Zihlmann [e], Niklaus Stiefel [e], Luigi Ambrosio [d], Jos Malda [c,f], Riccardo Levato [c,f], José Crecente-Campo [a,b,*], María José Alonso [a,b,*]

[a] Center for Research in Molecular Medicine and Chronic Diseases (CIMUS), IDIS Research Institute, Universidade de Santiago de Compostela, Santiago de Compostela, Spain
[b] Department of Pharmacology, Pharmacy and Pharmaceutical Technology, School of Pharmacy, Campus Vida, Universidade de Santiago de Compostela, Santiago de Compostela, Spain
[c] Department of Orthopaedics, University Medical Center Utrecht, Utrecht, the Netherlands
[d] Institute of Polymers, Composites and Biomaterials, National Research Council (IPCB-CNR), Naples, Italy
[e] Geistlich Pharma AG, Wolhusen, Switzerland
[f] Department of Clinical Sciences, Faculty of Veterinary Medicine, Utrecht University, Utrecht, the Netherlands

ARTICLE INFO

Keywords:
Anti-angiogenic effect
Protein delivery
PLGA
3D printing
Cartilage
meniscus

ABSTRACT

Pathological angiogenesis is a crucial attribute of several chronic diseases such as cancer, age-related macular degeneration, and osteoarthritis (OA). In the case of OA, pathological angiogenesis mediated by the vascular endothelial growth factor (VEGF), among other factors, contributes to cartilage degeneration and to implants rejection. In line with this, the use of the anti-VEGF bevacizumab (BVZ) has been shown to prevent OA progression and support cartilage regeneration. The aim of this work was to functionalize a medical grade collagen with poly (lactic-*co*-glycolic acid) (PLGA) microparticles containing BVZ *via* three-dimensional (3D) printing to target pathological angiogenesis. First, the effect of several formulation parameters on the encapsulation and release of BVZ from PLGA microparticles was studied. Then, the anti-angiogenic activity of released BVZ was tested in a 3D cell model. The 3D printability of the microparticle-loaded collagen ink was tested by evaluating the shape fidelity of 3D printed structures. Results showed that the release and the encapsulation efficiency of BVZ could be tuned as a function of several formulation parameters. In addition, the released BVZ was observed to reduce vascularization by human umbilical vein endothelial cells. Finally, the collagen ink with embedded BVZ microparticles was successfully printed, leading to shape-stable meniscus-, nose- and auricle-like structures. Taken altogether, we defined the conditions for the successful combination of BVZ-loaded microparticles with the 3D printing of a medical grade collagen to target pathological angiogenesis.

1. Introduction

Pathological angiogenesis is a crucial attribute of cancer and several chronic inflammatory diseases, such as age-related macular degeneration (AMD) and osteoarthritis (OA) [1,2]. In cancer, new vessels develop by sprouting from pre-existing vessels leading to an abnormal vasculature with a disorganized architecture and a high vascular permeability, among other features [1]. In AMD, a chronic retinal disease, new abnormal vessels originating from the vascularized choroid invade the retinal space, leading to death of photoreceptors and irreversible blindness [2]. More recently, pathological angiogenesis has also been linked to OA, a chronic inflammatory disease characterized by the damage of the articular cartilage, pain, and reduced mobility. The association between pathological angiogenesis and OA has emerged

* Corresponding authors at: University of Santiago de Compostela (USC), Av. Barcelona s/n Campus Vida, 15706 Santiago de Compostela, Spain.
E-mail addresses: anna.abbadessa@usc.es (A. Abbadessa), P.NunezBernal@umcutrecht.nl (P. Nuñez Bernal), giorgio.buttitta@rai.usc.es (G. Buttitta), alfredo.ronca@cnr.it (A. Ronca), ugo.damora@cnr.it (U. D'Amora), carla.zihlmann@geistlich.com (C. Zihlmann), Niklaus.Stiefel@geistlich.com (N. Stiefel), luigi.ambrosio@cnr.it (L. Ambrosio), J.Malda@umcutrecht.nl (J. Malda), R.Levato-2@umcutrecht.nl (R. Levato), jose.crecente@usc.es (J. Crecente-Campo), mariaj.alonso@usc.es (M.J. Alonso).
[1] Present address: Department of Drug Chemistry and Technologies, Sapienza University of Rome, Rome, Italy

https://doi.org/10.1016/j.jconrel.2023.07.017
Received 17 February 2023; Received in revised form 5 June 2023; Accepted 8 July 2023
Available online 19 July 2023

following the observation that OA patients present vasculature in the articular cartilage and in the inner meniscus, which normally are avascular structures [3].

As in cancer and in AMD, also in OA, members of the vascular endothelial growth factor (VEGF) family play a key role, among other factors [1,3]. In OA, this angiogenetic process is associated to a progressive breakdown of the extracellular matrix (ECM) and tissue degeneration [3,4]. In fact, one of the effects of VEGF is the stimulation of the degrading enzymes matrix metalloproteinases (MMPs) and the inhibition of the tissue inhibitors of the matrix metalloproteinases (TIMP) [4,5]. Moreover, the VEGF-mediated cellular invasion can cause premature resorption of implanted cartilage scaffolds *in vivo*, *via* monocyte chemoattraction [6]. These observations highlight the importance of modulating the VEGF activity during OA and when a scaffold-mediated regeneration of avascular cartilage and fibrocartilage is sought.

Bevacizumab (BVZ) is a full-length, humanized, recombinant monoclonal antibody against all isoforms of VEGF-A. It was approved by the Food and Drug Administration (FDA) for the treatment of the advanced stage of colon, lung, kidney, and brain cancers, and it is also used as an off-label drug for the treatment of AMD [7,8]. Recently, BVZ has also emerged as a promising active factor to block pathological angiogenesis and support regeneration in OA cartilage [9–11]. As an example, BVZ was reported to support the repair of articular cartilage in an osteochondral defect model in rabbits [12]. Moreover, BVZ was found to preserve scaffold long-term stability *in vivo* [6]. Despite these promising *in vivo* results, the incorporation of BVZ in three-dimensional (3D) printed scaffolds for their use in regenerative medicine has not been explored yet.

In this study, we biofunctionalized a medical grade collagen with BVZ-loaded microparticles to target pathological angiogenesis as that found in OA cartilage and meniscus. Moreover, we tested the processability of this composite material *via* 3D printing, a widely explored technology for the fabrication of customized scaffolds in tissue engineering. The rationale behind the use of polymeric microparticles is the prevention of the premature degradation of BZV and its controlled release upon implantation of the scaffolds [13]. In this sense, it has been argued that for the efficient VEGF blockage in the context of OA cartilage, it would be important to achieve a continuous delivery of BZV for 2–3 weeks [6,12]. To achieve such profile, we selected microparticles made of poly(lactic-*co*-glycolic acid) (PLGA), a polymer known for its capacity to control the release of biological drugs, including BVZ [14–21].

In our study, a medical grade porcine collagen material that has already been applied in clinical procedures for cartilage, bone regeneration and wound healing [22–26] was selected for the production of the scaffold using 3D printing. This technique was selected because it allows the design and manufacturing of customized complex structures by the layer-by-layer deposition of printable materials, *i.e.*, inks, that may carry cells and active factors [27–32]. Remarkably, 3D printing allows for the spatial distribution of these elements to recreate naturally occurring gradients, as those present in the articular cartilage and meniscus [33,34]. For example, the human meniscus presents an outer vascularized zone (the red zone) that gradually turns into an avascular inner zone (the white zone, outer-inner gradient), whereas articular cartilage is avascular and presents several horizontal zones that differ in terms of cell morphology and density, as well as in the content and arrangement of the ECM components (bottom-up gradient). For such anisotropic tissues, 3D printing can allow a spatio-specific distribution of active factors throughout tissue-engineered scaffolds to mimic zone-specific features. This can be important to recreate an appropriate milieu for cell differentiation and tissue ingrowth [34,35].

Taken altogether, we combined BVZ micro-encapsulation and 3D printing to fabricate medical grade scaffolds loaded with anti-angiogenic microparticles targeting pathological angiogenesis, as that found in OA cartilage and meniscus. Remarkably, this approach may be potentially extended to other diseases with pathological angiogenesis, such as cancer and AMD.

2. Materials and methods

2.1. Materials

Ester-terminated PLGA (capped PLGA) Resomer® RG 502 25G (D,L-Lactide:Glycolide ratio = 50: 50, M_n = 6880 Da, M_w = 14,700 Da) and Resomer® RG 503 25G (D,L-Lactide:Glycolide ratio = 50: 50, M_n = 12,100 Da, M_w = 35,800 Da) were supplied by Evonik. Polyvinyl alcohol (PVA) was purchased by Nippon Gohsei, whereas poloxamer 184 (Pluronic® L64) and kolliphor® HS 15 were supplied by BASF. Dichloromethane (DCM), dimethylsulphoxide (DMSO) and sodium azide were purchased by Scharlau, whereas phosphate-buffer saline (PBS) was purchased from Fischer Scientific. The anti-angiogenic BVZ (Avastin®) was kindly donated by mAbxience-GH Genhelix. Recombinant human VEGF 165 was supplied by Peprotech, goat anti-human IgG horseradish peroxidase (HRP)-conjugated by Jackson ImmunoResearch and sodium hyaluronate (molecular weight = 290 kDa) by Bloomage Biotech. Tween® 80 and Tween® 20 were purchased from Merck, and 2,2′-azino-di-(3-ethylbenzthiazoline sulfonic acid) (ABTS) from Roche. Green fluorescent protein-expressing human umbilical vein endothelial cells (GFP-HUVECs) were supplied by Angio-Proteomie (USA). Endothelial Growth Medium-2 (EGM-2) and Endothelial Basal Medium-2 + SingleQuots were purchased from Lonza (The Netherlands), whereas Dulbecco Modified Eagle Medium (DMEM) + GlutaMAX (31966), fetal bovine serum (FBS, 10% *v*/v, 10,270), penicillin/streptomycin (p/s 1%) and N-2-hydroxyethylpiperazine-N-2-ethane sulfonic acid (HEPES, 15630080) from Gibco (The Netherlands). Fibrinogen (F8630) and thrombin (T4648) were supplied by Sigma-Aldrich, bovine serum albumin by Roche, resazurin sodium salt by Alfa Aesar (Germany). Porcine, decellularized medical-grade collagen composed of collagen type I, type III and elastin, and purified as described in the patent BioGide (EP1676592) was donated by Geistlich Pharma AG (Wolhusen, Switzerland). All other chemicals were supplied by Sigma-Aldrich.

2.2. Experimental design

Firstly, a formulation study was carried out to identify the parameters that allow the fabrication of BVZ-loaded microparticles with high encapsulation efficiency (EE) and with a BVZ sustained release over the first 21 days. Secondly, two selected formulations were tested *in vitro* in a 3D vascularization model to study the anti-angiogenic activity of released BVZ and its effect on cellular metabolic activity. Thirdly, we studied the effect of microparticles on the 3D printability of a medical grade collagen ink and evaluated the feasibility of fabricating complex structures.

2.3. Preparation of BVZ-loaded microparticles

Microparticles composed of capped PLGA were prepared according to the water-in-oil-in-water double emulsion-solvent evaporation method as previously reported [36], with some modifications. The detailed protocol used in the formulation screenings 1 and 2 is reported in Supporting Information (Section 1). The formulation parameters used as variables are reported in Tables 1 and 2. The encapsulation efficiency (EE), defined as the percentage of entrapped protein *versus* total protein, was calculated using either a direct method or an indirect method, as reported in Supporting Information (Section 2).

2.4. In vitro release study

Microparticles were dispersed in PBS (5 mg/mL) enriched with sodium azide and Tween® 20 (further referred to as release medium) and incubated at 37 °C under mild agitation. At predefined time intervals,

Table 1
Effect of surfactants and their concentration in the organic phase on the BZV encapsulation efficiency (EE) of PLGA microparticles (formulation screening 1).

Sample	Surfactant in the organic phase	Surfactant concentration (mg/mL)	Average diameter (μm)	EE (%)
S1-PF50	Pluronic® F-68 (HLB = 28.0)	50	6.5 ± 7.4	53 ± 3
S1-PL150	Pluronic® L-64 (HLB = 15.0)	150	1.5 ± 0.3	48 ± 3
S1-TW25	Tween® 80 (HLB = 15.0)	25	2.3 ± 0.7	39 ± 0
S1-TW50		50	2.5 ± 1.3	22 ± 2
S1-SP50	Span® 60 (HLB = 4.3)	50	2.7 ± 1.4	83 ± 4

The concentration of BVZ in the inner water phase (w1) was 28.9 mg/mL (0.2 mL), the concentration of capped PLGA (14 kDa) in the organic phase was 50 mg/mL (1 mL). In the abbreviations, S1 indicates screening 1, and the last 4 characters refer to the name of the surfactant and concentration used. Standard deviation values of the average diameter indicate particle size variability within a given batch.

Table 2
Effect of the PLGA/BVZ and Tween® 80/BVZ ratios on the encapsulation efficiency (EE) and microparticle size (formulation screening 2).

Sample	Volume w1 (mL)	PLGA concentration (mg/mL)	PLGA/BVZ ratio	TW80/BVZ ratio	Average diameter (μm)	EE (%)
S2-PB50	0.1	250	50	2.3	107 ± 57	93 ± 7
S2-PB25a	0.2	250	25	2.3	81 ± 35	82 ± 1
S2-PB25b	0.1	125	25	2.3	39 ± 13	78 ± 8
S2-PB12	0.2	125	12.5	2.3	55 ± 21	75 ± 2
S2-PB7a	0.2	75	7.5	2.3	53 ± 22	62 ± 8
S2-PB7b	0.2	75	7.5	4.6	42 ± 21	85 ± 1

Different PLGA/BVZ ratios were obtained by varying the volume of the primary water phase w1 (fixed BVZ concentration = 25 mg/mL) and the concentration of capped PLGA (36 kDa) in the organic phase (fixed volume = 500 μL), whereas different Tween® 80/PLGA ratios were obtained by varying the concentration of Tween® 80 (58 or 116 mg/mL) in w1. In the abbreviation, S2 indicates screening 2 and PB indicates the PLGA/BVZ ratio. For the formulations PB25, a and b indicate that the same PLGA/BVZ ratio was achieved using different volumes of w1 and different concentrations of PLGA in the organic phase; whereas for the formulations PB7, a and b indicate that the formulations have a different Tween® 80/BVZ ratio. Standard deviation values of the average diameter indicate particle size variability within a given batch.

microparticles were centrifuged at 4 °C for 30 min using a speed of 10,000 *g* (Centrifuge 5430R Eppendorf, formulation screening 1) or precipitated by sedimentation (formulation screening 2). Supernatants were taken and analysed for protein quantification. The pellets were resuspended in fresh release medium and incubated as explained above. The released BVZ at each time point was quantified by a Bradford protein assay according to the manufacturer's protocol. Calibration curves were obtained using freshly prepared solutions of BVZ in the release medium, and by reading the absorbance at 595 and 466 nm by a Synergy H1 Hybrid Multi-Mode Reader (BioTeck). The ratio between the 2 absorbance values was used to build the calibration curve and to calculate BVZ concentration in the samples. For selected formulations, the released BVZ at different time points was also quantified by an enzyme-linked immunosorbent assay (ELISA), according to a protocol reported in the Supporting Information (Section 3).

2.5. Particle size and morphology

Microparticles were visualized by using an Olympus IX51 optical microscope, equipped with an Olympus DP72 camera. The samples were prepared by placing 10 μL of a particle suspension (5 mg/mL) on a microscope slide and covered by a coverslip. The average particle diameter was determined by measuring the circumference of at least 70 microparticles, with an Olympus cellSens standard 1.16 software according to a 3-point circle identification method. Microparticle morphology of selected formulations was studied using Field Emission Scanning Electron Microscopy (FESEM). To this end, a volume of 25 μL of a microparticle suspension (5 mg/mL) was deposited on a silicon wafer previously attached on top of a carbon-taped aluminium stub. Microspheres were air-dried overnight and then sputter-coated with a 5-nm coating of Iridium. Finally, microparticles were visualized using a FESEM microscope (Ultra plus FESEM, ZEISS), in a regime of high void.

2.6. Cell isolation and culture

GFP-HUVECs were used in co-culture with human bone marrow-derived mesenchymal stromal cells (hbMSCs) to evaluate the anti-angiogenic effect of selected formulations of BVZ-loaded microparticles. hbMSCs were isolated from bone marrow aspirates obtained from consenting patients as previously described [37]. The procedures to isolate human tissue and cells were approved by the research ethics committee of the University Medical Center Utrecht. GFP-HUVECs were cultured in EGM-2 medium containing Endothelial Basal Medium-2 + SingleQuots, 100 U/mL-100 μg/mL PenStrep, and 10% heat-inactivated FBS. HbMSCs were cultured in DMEM + GlutaMAX supplemented with FBS (10% *v*/v) and p/s 1%. All cells were cultured at 37 °C and 5% CO_2.

2.7. Casting of GFP-HUVECs and hbMSC-laden fibrin gels

GFP-HUVECs and hbMSCs co-cultures were embedded in 3D fibrin gel droplets consisting of 6.6 mg/mL of fibrinogen and 2 U/mL of thrombin. GFP-HUVECs were encapsulated at a density of 2.5×10^6 cells/mL of gel and hbMSCs were encapsulated at a density of 5×10^6 cells/mL of gel. To this end, the cell pellet was suspended in fibrinogen dissolved in saline supplemented with 1% *w/v* bovine serum albumin and 10 mM HEPES. The cell-laden fibrinogen solution was then mixed with thrombin dissolved in DMEM supplemented with p/s. Fibrin gel droplets of a volume of 20 μL were casted directly on the surface of a culture plate and incubated for 20 min at 37 °C to allow complete gelation. The droplets were cultured in EGM-2 medium for 7 days in the presence of fibrin-encapsulated blank or BVZ-loaded microparticles (10 mg of microparticles/60 μL of fibrin gel) or BVZ-supplemented medium (10 μg/mL) (Fig. 4a). Medium was refreshed every 2 days. Two formulations of BVZ-loaded microparticles were tested, namely S1-PL150 and S2-PB7b, that were selected from the formulation screenings 1 and 2, respectively.

2.8. Evaluation of cell metabolism and anti-angiogenic activity

Metabolic activity of cell-laden droplets cultured in the presence of free BVZ, BVZ-loaded, and blank microparticles was assessed through a resazurin assay after 1 and 7 days in culture (n = 4–6). Cell-laden droplets cultured in the presence of free BVZ, BVZ-loaded, and blank microparticles were evaluated for their angiogenic capacity after 7 days

in culture (n = 4–6). Samples were fixed in 4% *v*/v neutral buffered formalin, and fluorescent images of the GFP-HUVEC networks were acquired using a Thunder imaging system (Leica Microsystems, Germany). The vessel area coverage, average vessel length and junction number were calculated using the vessel analysis software AngioTool [38].

2.9. Preparation of the blank and microparticle-loaded collagen ink

A blank collagen ink was prepared by dissolving medical-grade collagen in PBS at 12.5% (*w*/w). The mixture was manually stirred with a spatula and the pH was lowered to 3.5 using ortho-phosphoric acid 85% to yield a smooth slurry. The slurry was further homogenized using a static mixer and finally centrifuged to remove air bubbles. For the preparation of the microparticle-loaded collagen ink, BVZ-loaded microparticles of a selected formulation, namely S1-PL150, were dispersed in the exact weight of PBS to obtain a final particle concentration of 4% (w/w) referred to the total slurry. The particle suspension was gently mixed for 10 s, added to the collagen powder, and further homogenized as explained above for the blank collagen ink. Before 3D printing, the ink was heated up to 30 °C for at least 10 min.

2.10. Assessment of 3D printability

The 3D printability of the microparticle-loaded collagen ink was compared to that of the blank collagen ink in a filament collapse and a filament fusion test [39]. For the filament collapse test, a platform with pillars (l × w × h = 2.0 × 2.0 × 4.0 mm^3) placed at known gap distances (1.0, 2.0, 4.0, 8.0, and 16.0 mm) was fabricated using a Perfactory Mini digital light projection 3D printer (Envisiontec, Germany) as previously reported [39]. Over these gaps, a single gel filament was deposited using a Rokit Invivo 4D2 bioprinter (Rokit Healthcare Inc., South Korea) equipped with a syringe dispenser and a 1.80 firmware. To this aim, the blank or the microparticle-loaded collagen ink was loaded into a Luer-Lock glass syringe (10 mL) with an inner diameter of 15.5 mm and extruded using a 0.61 mm needle (GA 20), a deposition speed of 4 mm/s, a layer thickness of 0.4 mm and a printing temperature of 25 °C. In the filament fusion test, three different patterns were used, each one corresponding to a specific infill of 50%, 70% and 90%. From the GCode analysis, it was found that the filament distances for the proposed infill of 50%, 70% and 90% were 0.60, 0.27 and 0.06 mm, respectively. To perform the fusion test of the blank and the microparticle-loaded collagen ink, the same printing parameters of the filament collapse test were employed. Top-down pictures were obtained using a Nikon digital camera directly after printing, as no apparent deformation was observed at this time point.

2.11. Microparticle distribution and 3D printing of anatomically shaped structures

To analyze the microparticle distribution throughout the 3D printed collagen scaffolds, rectangular cuboids (13 × 13 × 5 mm) with an infill of 70% were fabricated using a Rokit Invivo 4D2 bioprinter. To this end, either the microparticle-loaded ink, or the blank collagen ink (as control), was loaded into a Luer-Lock glass syringe and 3D printed using the printing parameters reported in Section 2.10. The input print pattern was sliced using a NewCreatorK 1.57.70 software. To preserve structural stability, the obtained samples were immersed in an aqueous solution of NaCl (100 mg/mL) for 1 h, washed three times in PBS for 2 h, and pH-adjusted to 7.4. Subsequently, samples were freeze-dried and chemically crosslinked with 1-Ethyl-3-(3-dimethylaminopropyl)carbodiimide (EDC) and *N*-hydroxysuccinimide (NHS) as described in the patent US2016166737A1. After cross-linking, washing steps in phosphate buffer at elevated pH and subsequent flushing steps were applied. Importantly, these steps allow the full inactivation of EDC and NHS, and permit to wash out remaining degradation products. Finally, samples were freeze-dried, conditioned at 22 °C and at 55% of relative humidity for 2 h, and sterilized by the company STERIS (Däniken, Switzerland) using X-ray irradiation at 22–33 kGy. Slices (thickness = 1 mm) of freeze-dried samples were fixed on top of a carbon-taped aluminium stub, sputter-coated with a 5 nm coating of Iridium and visualized by a FESEM, as reported in Section 2.5 for the visualization of microparticles. Finally, to show the feasibility of a clinically relevant printing process, complex anatomically shaped structures resembling the human meniscus, nose and auricle were printed based on generic models with a 70% infill.

2.12. Statistics

Results were reported as mean ± standard error of the mean (S.E.M.). Statistical analysis of vessel network characterization and cellular metabolic activity was performed using GraphPad Prism 9.0 (GraphPad Software, USA). Comparisons between experimental groups were assessed *via* one- (vessel network characterization) or two-way (metabolic activity) ANOVAs, followed by *post hoc* Bonferroni correction to test differences between groups. Normality was checked with a Shapiro-Wilk test. Differences were found to be significant when $p < 0.05$.

3. Results and discussion

3.1. Characterization of BVZ-loaded PLGA microparticles

3.1.1. Effect of surfactants in the organic phase on the encapsulation and release of BZV from PLGA microparticles - formulation screening 1

First, an explorative screening (16 formulations) involving different non-ionic surfactants at different concentrations and in combination with two different PLGA molecular weights (Section 4, Table S1 and Fig. S1, Supporting Information) was carried out. From this study, the five most interesting formulations in terms of EE and release profile were selected for the formulation screening 1 (Table 1). In this screening, the effect of different surfactants (Pluronic® F-68, Pluronic® L-64, Tween® 80 and Span® 60), used at different concentrations, was investigated.

The EE values presented a broad range (22–83%) as a function of the surfactant hydrophilic/lipophilic balance (HLB). This can be appreciated by comparing the formulations S1-PF50, S1-TW50 and S1-SP50, prepared using the same concentration in the organic phase of three different surfactants with different HLB values, *i.e.*, Pluronic® F-68 (HLB = 28.0), Tween® 80 (HLB = 15.0) and Span® 60 (HLB = 4.3), respectively. Formulations prepared with Span® 60 showed the highest values of EE, *i.e.*, 83%. This finding is in line with the results reported in previous literature, where the high encapsulation of hydrophilic drugs into poly(D,L-lactide) (PLA) and PLGA microspheres in the presence of Span® 60 was attributed to the low HLB of this surfactant, which makes it an ideal stabilizing agent for water-in-oil interfaces [40,41]. By increasing the HLB from 4.3 (Span® 60) to 15.0 (Tween® 80), the EE values dramatically decreased down to 22%. By further increasing the HLB to 28.0 (Pluronic® F-68), the EE values increased again up to 53%. This trend is in line with the observations by Dinarvand et al. regarding the encapsulation of a hydrophilic drug into PLA microparticles [40]. The lower EE found for the formulations made with Tween® 80 can be attributed to its higher HLB, as compared to that of Span® 60 and, therefore, to its inferior capacity for the stabilization of the primary emulsion (w1/o). On the other hand, the moderate EE values found for the formulations made with the most hydrophilic surfactant of the study, *i.e.*, Pluronic® F-68 demonstrated that the EE can also benefit from the stabilization of the secondary emulsion (o/w2), mediated by the migration of these surfactants to the o/w2 interface, which reduces the amount of protein adsorbed onto the microparticles surface [40]. Moreover, surfactants with high HLB may interact with the PVA present in the outer water phase, forming a gel-like stabilizing barrier [40].

Previous studies reported in literature have shown that the EE values of BVZ into PLGA nano- and microparticles fabricated by the double

emulsion technique are usually higher than 80% [18,19,42,43]. However, it must be noted that in these studies uncapped PLGA is used, for which we have also found similarly high values of EE (Section 5, Supporting Information). These high values of EE are likely due to the electrostatic interactions between the positively charged BVZ and the negatively charged PLGA carboxyl end groups. In this study, we preferred the use of capped PLGA, since the uncapped polymer did not support the desired release kinetics (Section 5, Supporting Information).

The BVZ release profiles of the tested formulations significantly differed as a function of the surfactant HLB and concentration (Fig. 1a and b). Formulations made with poloxamers (Pluronic® F-68 and Pluronic® L-64) showed a release kinetics, characterized by an initial burst release phase during the first 2–3 days followed by a slower release until day 21. These formulations showed the lowest burst release (percentage of BVZ released by day 2 was 11% and 15%, for S1-PF50 and S1-PL150, respectively) and the lowest total percentage of BVZ released by day 21 (16% and 22% for S1-PF50 and S1-PL150, respectively). Overall, the burst release of BVZ increased when the surfactant HLB decreased. This can be appreciated by comparing the formulations S1-PF50, S1-TW50 and S1-SP50, which organic phases contain the same concentration of three different surfactants with different HLB values, *i.e.*, Pluronic® F-68 (HLB = 28.0), Tween® 80 (HLB = 15.0) and Span® 60 (HLB = 4.3), respectively. Indeed, the percentage of BVZ released by day 2 was 11%, 29%, and 39%, for S1-PF50, S1-TW50 and S1-SP50, respectively. This trend can be explained by considering the different distribution of the surfactant and the protein within the PLGA matrix. Surfactants with a low HLB tend to position themselves preferentially toward the oily PLGA-containing phase, whereas those with a high HLB tend to diffuse toward the water phase, which causes a correspondent displacement of the entrapped protein [40]. Therefore, in the former case, the fraction of the protein that the surfactant displaces from the core and that ends up onto the microparticle surface is much higher. This explains the much higher burst release of BVZ observed when using surfactants with a lower HLB. The formulation S1-SP50 showed the highest burst release and the highest value of total BVZ released by day 21 (*i.e.*, 41%), however between day 5 and day 21 only a minor percentage of BVZ was released, which could be due to the absence of release or to the degradation of the protein molecules. S1-PL150 was the best performing formulation in terms of providing a constant release of BVZ from day 5 to day 21 (distributive release profiles shown in Fig. S3, Supporting Information) and, hence, was selected for further evaluation by ELISA and by cellular *in vitro* studies.

It must be noted that all formulations exhibited incomplete release of BZV, a result in line with previously reported data on the release of BVZ from PLGA particles [14,18,19]. For instance, Sousa et al. reported a total 15% BZV release over the first 7 days [19]. A low amount of total BZV release (< 10%) was also observed by Varshochian et al. during the first 21 days [18]. This incomplete protein release often noted for PLGA particles has been found to be dependent on the protein isoelectric point and protein size, as well as on the PLGA charge density and particle porosity [19]. The incomplete release of BVZ observed in our study is likely due to protein/polymer interactions, as previously described for protein-loaded PLGA particles [44–47]. Indeed, all formulations showed an insoluble residue at the end of the study. The presence of a residue originated by protein/polymer interactions has been previously reported for PLGA microparticles [45]. To understand the role of BVZ on the generation of this residue, in a separate experiment, BVZ-loaded and blank microparticles made with a fast-degrading uncapped PLGA with a molecular weight of 2 kDa were prepared and monitored for 21 days. This PLGA type was selected because a complete PLGA degradation was expected during 21 days. This is important to exclude that the residue generation was due to undegraded PLGA matrix. Importantly, BVZ-loaded formulations showed an insoluble residue at day 21, whereas no residue was observed for the blank formulations (Fig. S4, Supporting Information). This confirms that the presence of BVZ into PLGA microparticles triggered the formation of insoluble complexes. In this context, an interesting aspect is to analyze whether these BVZ/PLGA interactions are established during the formulation process or also after that BVZ has

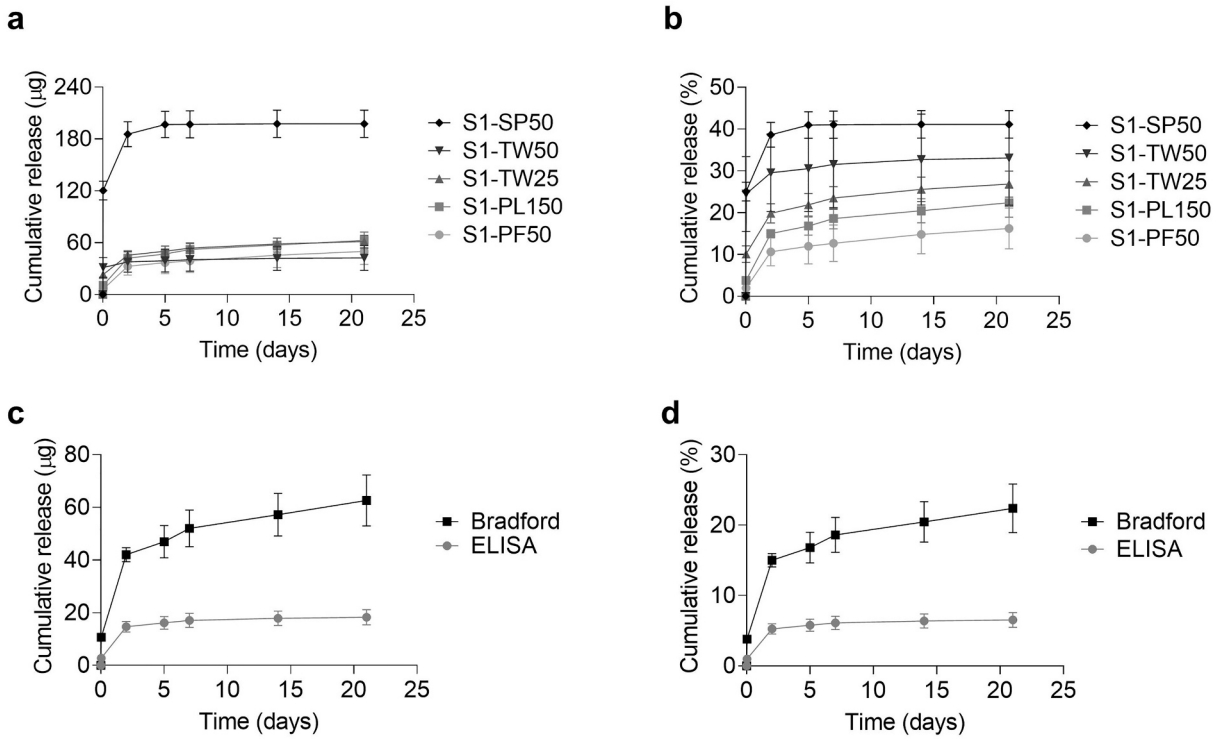

Fig. 1. BVZ release profiles of the formulations prepared in the formulation screening 1. BZV cumulative release of all formulations in µg (a) and % (b) as a function of time. BVZ release profiles according to the Bradford assay and ELISA of the formulation S1-PL150. Cumulative release in µg (c) and % (d) as a function of time. In the abbreviations, S1 indicates screening 1, whereas the last 4 characters refer to the name of the surfactant and to the concentration used (Table 1).

been released (post-release BVZ adhesion onto PLGA residual particles). To answer this question, a separate experiment was performed. BVZ was dissolved in the release medium, incubated with blank microparticles, and free BVZ in the supernatant was quantified at day 0 and 7. No significant adhesion of BVZ was observed in this experiment. Therefore, the observed incomplete release cannot be attributed to post-release BVZ-PLGA interactions, but to an actual lack of BVZ release due to protein-polymer interactions that occur during the formulation and incubation process.

ELISA/Bradford comparative studies allowed to quantify the active protein (ELISA quantification) as a percentage of the total protein released (Bradford quantification, Fig. 1c and d). These studies showed that the percentage of active protein for the selected formulation (namely, S1-PL150) ranged between 26 and 35%, depending on the time point under consideration. The partial protein inactivation observed in our study is in line with the results of Varshochian et al. who reported a protein inactivation of up to 79% during the first 21 days in an *in vitro* release study [18]. Importantly, the same authors found a much higher amount of active protein released in an *ex-vivo* model. This highlights the intrinsic limitations of *in vitro* release studies and the need to complement *in vitro* release data with other protein activity assays, as we illustrate in Section 3.2.

3.1.2. *Effect of the PLGA/BVZ and tween® 80/BVZ ratios on the encapsulation and release of BZV from PLGA microparticles - formulation screening 2*

The aim of the formulation screening 2 was to study the effect of the PLGA/BVZ ratio and the Tween® 80/BVZ ratio on the EE and release kinetics when the surfactant is dissolved in the primary water phase (w1) (Table 2). In this screening, Tween has been preferred over Pluronic because, according to the literature, it has been previously mixed in aqueous phases for BVZ micro- and nanoencapsulation, with a beneficial effect on the EE and stability [48,49]. Span has been excluded due to its insolubility in water.

The EE presented values between 62 and 93%, depending on the composition (Table 2). Overall, the EE increased when the PLGA/BVZ ratio increased. This general trend is in agreement with the results reported previously regarding protein delivery from PLGA microparticles [21], and can be explained by the fact that an increase in the PLGA/BVZ ratio implies a lower BVZ diffusion from the internal water phase to the external one due to a lower BVZ gradient. Moreover, in our study an increase in the PLGA/BVZ ratio was also obtained by increasing the PLGA concentration, which causes an increase in the viscosity of the organic phase that, in turn, reduces the BVZ diffusion toward the external water phase [21]. Furthermore, by increasing the PLGA concentration, bigger particles were obtained. This likely caused a decrease in the BVZ leakage due to the relatively lower superficial area of bigger particles.

By comparing the formulations S2-PB7a and S2-PB7b, it can be noted that an increase in the TW80/BVZ ratio from 2.3 to 4.6 caused a significant increase in the EE (from 62 to 85%). This is in line with the findings reported by Narayana et al., who also found higher EE by increasing Tween 80 concentration [48]. Overall, the values of EE in the formulations of the screening 2 (Table 2) were higher than those found in the formulation screening 1 (Table 1), likely due to the bigger particle size (40–100 μm *vs* 1–5 μm) and the milder homogenization used in the formulation screening 2.

All formulations showed a sustained release of BVZ during the first 21 days (cumulative release curves in Fig. 2 and distributive release curves in Fig. S5, Supporting Information). In line with previously reported data on BVZ release from PLGA particles, the release was accelerated by decreasing the PLGA/BVZ ratio (from 50 to 7.5) and by decreasing the particle size (from 100 to 40 μm) [14]. The formulation S2-PB7b, which had the lowest PLGA/BVZ ratio and the highest Tween® 80/BVZ ratio, released the highest amount of BVZ at day 21 (126 μg, 21%). This result indicates that the decrease in the PLGA/BVZ ratio and the increase in the Tween® 80/BVZ ratio had a synergistic effect in boosting BVZ release. For this reason, the formulation S2-PB7b was selected for further *in vitro* cellular studies. Remarkably, the percentage of active protein in the total released protein was higher than that found in the screening 1, ranging between 50 and 64% depending on the time point under consideration. Such difference is likely explained by the

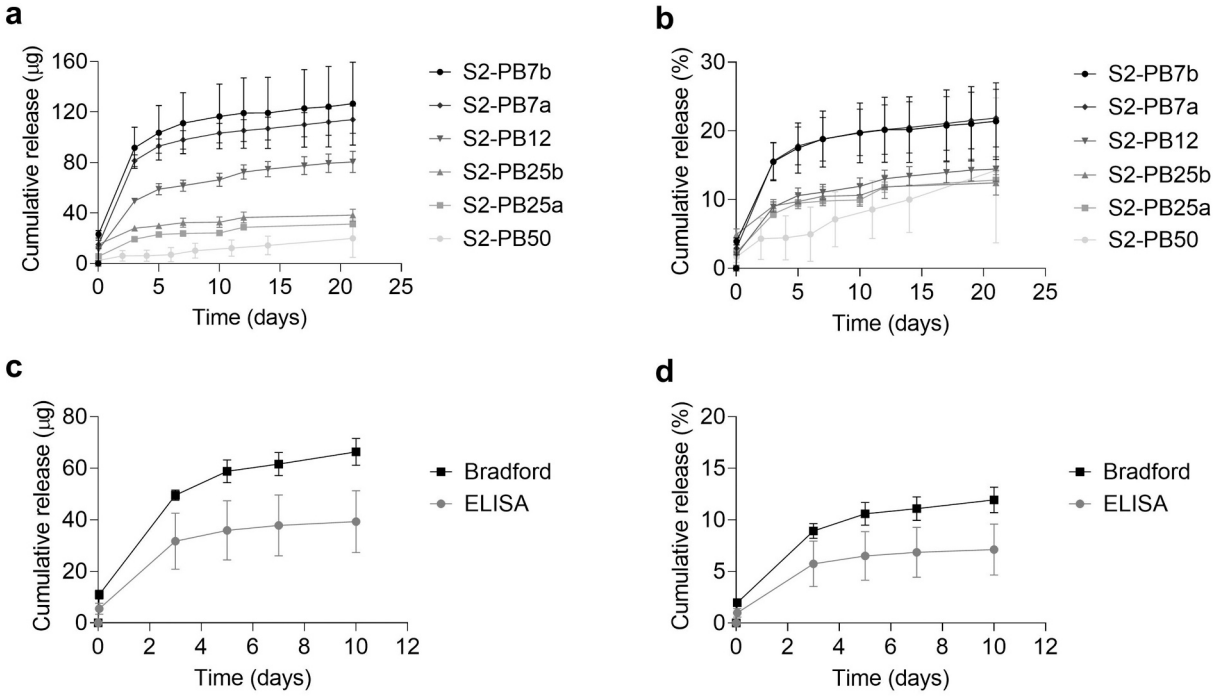

Fig. 2. BVZ release profiles of the formulations prepared in formulation screening 2. BZV cumulative release of all formulations in μg (a) and % (b) as a function of time. BVZ release profiles according to the Bradford assay and ELISA of the formulation S2-PB12. Cumulative release in μg (c) and % (d) as a function of time. In the abbreviations, S2 indicates formulation screening 2 and PB indicates the PLGA/BVZ ratio (Table 2).

milder homogenization procedure employed in the screening 2 compared to the screening 1 (vortex at 2200 rpm *vs* Ultra Turrax 11,200 rpm), and a more protective role of the higher PLGA concentration and of the surfactant in the primary water phase used in the screening 2.

3.1.3. Morphology of BVZ-loaded microparticles

The formulations S1-PL150 and S2-PB7b, selected for the *in vitro* cellular studies, were also visualized by FESEM. The BVZ-loaded microparticles of the formulation S1-PL150 had a diameter of about 1 μm and presented a rougher surface and a less spherical shape than the blank microparticles prepared using the same method (Fig. 3a and b). This result indicates that the presence of BVZ affects the particle morphology, likely due to a partial BVZ/PLGA phase separation during solvent evaporation which causes dimples on the surface [14,50]. The appearance of the BVZ-loaded microparticles after 21 days of release study was very similar to the one of the microparticles at day 0 (Fig. 3c), which indicates that no visible particle degradation has occurred during that time frame.

BVZ-loaded microparticles from the formulation S2-PB7b had an average diameter of 40 μm, a spherical shape, and a rough and highly porous surface (Fig. 3d and e). We hypothesize that this high porosity is due to the lower PLGA/BVZ ratio and higher content of Tween® 80 used in this formulation compared to the other formulations prepared in the formulation screening 2. In line with this, BVZ-loaded microparticles of the formulation S2-PB50, which had the highest PLGA/BVZ ratio and the lowest amount of Tween® 80, showed a non-porous surface (Fig. 3f). The observed particle porosity further supports the higher burst release of BVZ from S2-PB7b compared to S2-PB50, as discussed in the Section 3.1.2.

3.2. In vitro cellular activity

In order to determine the bioactivity of the microencapsulated BVZ, the anti-angiogenic activity of the two selected microparticle formulations (namely, S1-PL150 and S2-PB7b) was tested on GFP-HUVEC and hbMSC-laden fibrin gels (Fig. 4a). This cellular co-culture has previously been shown to elicit HUVEC-driven network formation. This process is aided by the presence of hbMSCs that differentiate into pericytes and provide support to the forming capillary networks [37,51]. Fibrin gel was selected as a cell carrier due to the high reproducibility of its properties and the simple casting procedure that facilitates high throughput studies. Moreover, fibrin gels have previously shown an ability to support endothelial proliferation, cell attachment and migration, leading to the formation of capillary-like structures [52–54]. As opposed to 2D cell culture models, cell encapsulation in a 3D matrix can provide a more physiologically relevant environment that is more permissive for angiogenesis to occur [53].

Firstly, we identified the active dose range of BVZ (10–100 μg/mL) at which anti-angiogenic effects were initially observed within the cell-laden fibrin droplets (Fig. S6, Supporting Information). From there, and considering the BVZ release profile of the selected formulations, we deduced that an amount of 10 mg of microparticles/well would be appropriate to study the anti-angiogenic capacity of our two selected formulations, as well as their effect on cell metabolism over a 7-day culture (Fig. 4). The fluorescent images and corresponding software-based output images representing the vessels and junctions present in the fibrin gel show a clear recession of the HUVEC network in the presence of soluble BVZ (positive control) or BVZ-loaded microparticles compared to the BVZ-free controls consisting of blank microparticles and fibrin only (Fig. 4b).

The quantitative analysis of these images further supports this observation as it shows a statistically significant decrease in the average vessel area (approximately a 1.3-fold decrease, Fig. 4c), average vessel length (approximately a 2-fold decrease, Fig. 4d) and total number of cellular junctions (approximately a 2-fold decrease, Fig. 4e), when comparing the results obtained with BVZ *versus* the BVZ-free controls. Furthermore, the anti-angiogenic effect observed for both microparticle formulations confirms that a significant percentage of the released BVZ retains its activity. In fact, the effect of soluble BVZ that is supplemented to the medium with each media change (a cumulative amount of 80 μg BVZ throughout the culture period) does not show any significant variation compared to both BVZ-loaded microparticle formulations tested (expected cumulative release of active BVZ $\leq$ 100 μg) in either of the aforementioned vessel analysis outputs. This result is in line with previous research that showed the anti-angiogenic effect of released BVZ from different micro/nanoparticle studies [20,43,55]. These observations suggest that the gradual and sustained release of BVZ from microparticles is an effective strategy to achieve a controlled anti-

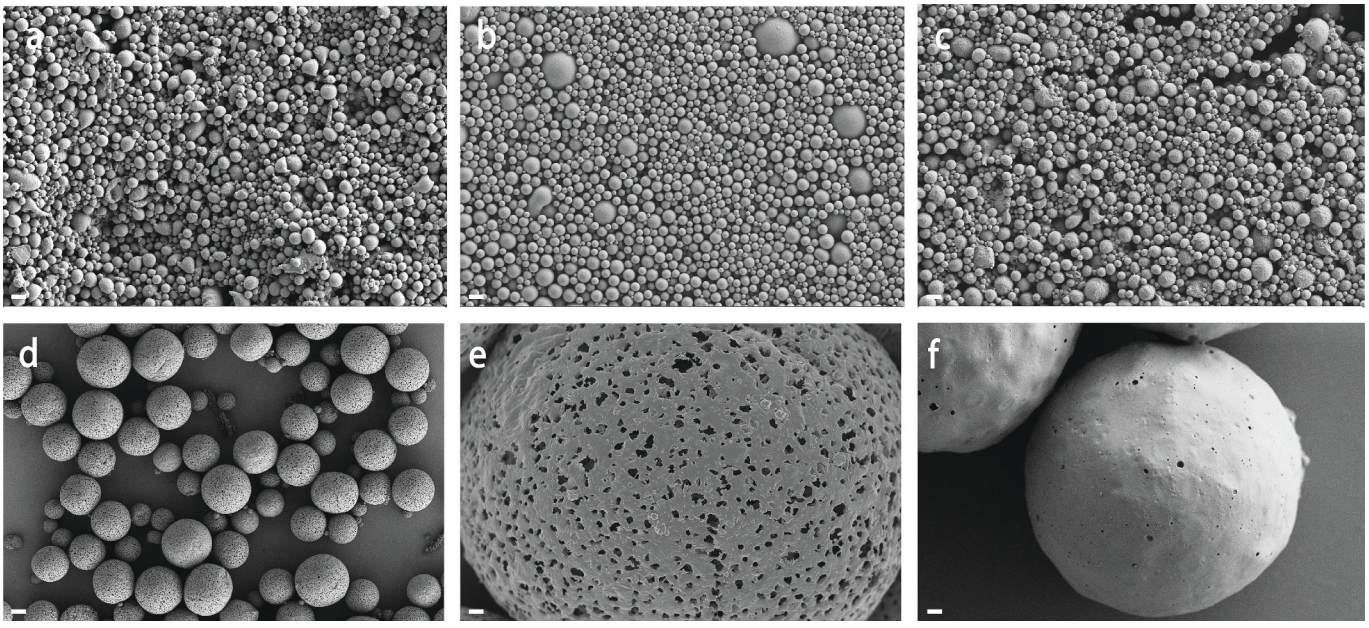

Fig. 3. FESEM images of microparticles. Formulation S1-PL150 (a-c). BVZ-loaded microparticles at day 0 (a), blank microparticles at day 0 (b), BVZ-loaded microparticles at day 21 (c). BVZ-loaded microparticles of the formulation S2-PB7b at day 0 (d-e). BVZ-loaded microparticles of the formulation S2-PB50 at day 0 (f). Scale bar is 2 μm for all photographs, except for the photograph d whose scale bar is 20 μm.

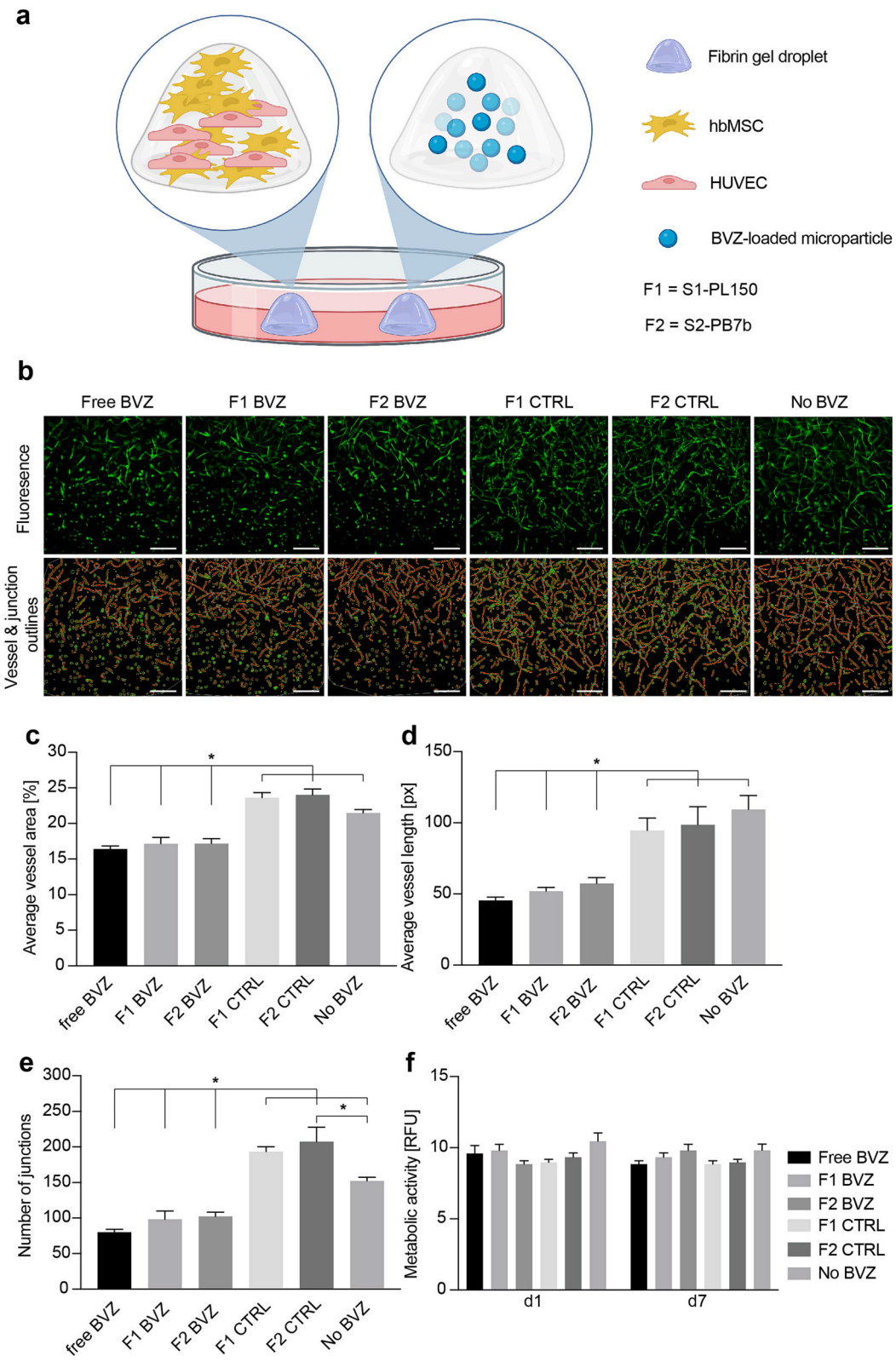

Fig. 4. Anti-angiogenic effect of BVZ-loaded microparticles on GFP-HUVECs and hbMSCs 3D co-culture model. Scheme of the *in vitro* model based on fibrin gel droplets loaded with GFP-HUVECs, hbMSCs and BVZ microparticles (a). Fluorescent images of the vascular networks formed by the GFP-HUVECs within the fibrin gels after 7 days in culture in the presence of free BVZ (cumulative amount of 80 μg/mL), two formulations of BVZ-loaded and blank microparticles (10 mg of microparticles/well), as well as BVZ-free controls (b, top panel). The AngioTool output diagrams showing the vessel outlines (red) and the cellular junctions (blue), scale bars = 250 μm (b, bottom panel). Average vessel area (c), average vessel length (d) and number of junctions of vascular networks (e) formed in the casted fibrin gels as calculated through the AngioTool software (n = 4–6) * = significant difference ($p < 0.05$). Metabolic activity of the 3D co-culture over a 7-day period, under the same experimental conditions (n = 4–6) * = significant difference ($p < 0.05$) (f). For simplicity, the two tested formulations S1-PL150 and S2-PB7b are referred to as F1 and F2, respectively. (For interpretation of the references to colour in this figure legend, the reader is referred to the web version of this article.)

angiogenic effect.

Importantly, despite the significant anti-angiogenic effect elicited by the introduction of BVZ in the co-culture system, neither the concentration, nor the way of BVZ supplementation (soluble BVZ supplemented to the media or BVZ released from microparticles) appeared to have a toxic effect on the established co-culture. Indeed, a constant metabolic activity (with values of fluorescence ranging from 8.8 to 10.4) was observed for all experimental conditions throughout the 7-day experiment. This observation is also in line with a previous study that employed similar BVZ concentrations (0.1–10,000 μg/mL) and showed no detrimental effect on HUVEC cell viability in the BVZ-concentration range used throughout the present study [20].

3.3. 3D printing of medical grade collagen biofunctionalized with BVZ-loaded microparticles

The cellular studies reported above (Section 3.2) showed a statistically comparable activity of the formulations S1-PL150 and S2-PB7b. Following this observation, the formulation S1-PL150 was used for further 3D printing studies for two technical reasons. Firstly, microparticles of the formulation S1-PL150 are more versatile for 3D printing applications because they have a smaller diameter than those of the formulation S2-PB7b (approx. 1 μm *vs* 40 μm, Section 3.1.3). Secondly, formulation S1-PL150 has a faster preparation protocol and easier handling.

To assess the 3D printability of the microparticle-loaded collagen ink, a filament collapse test and a filament fusion test were performed. In these tests, the filaments of the microparticle-loaded collagen ink were compared to those of the blank collagen ink (control). No filament collapse was observed after printing and over time for any of the two inks (*i.e.*, with and without microparticles, Fig. 5b), suggesting that the presence of BVZ-loaded microparticles at a concentration of 4.0% (*w*/w) did not affect the 3D printability of the collagen ink. The fact that no filament collapse was observed even at the highest gap distance of 1.6 cm, suggests that, if needed, an increase of particle concentration up to a certain extent could be implemented without expecting any detrimental effect on the 3D printability. This would allow, for example, an increase in the dose of BVZ/scaffold, if required by the specific application, animal model and implantation site in future studies. Results from the filament fusion test showed that for the two inks, there was a similar relationship between the infill increase and the filament gap closure (Fig. 5c). As reported in the Section 2.10, an increase in the infill density (input parameter controlled by the used software) from 50% to 90% resulted in a decrease of the line spacing in the printed pattern, and a clear filament fusion was observed only when using the highest infill value of 90%. For this reason, to ensure an adequate porosity, an infill value of 70% was considered the most appropriate for subsequent experiments.

The SEM imaging on cross-sections of 3D printed, chemically cross-linked collagen scaffolds containing BVZ-loaded PLGA microparticles showed a uniform distribution of the spherical microparticles in the scaffold (Fig. 5e and f). SEM images of cross-sections of blank 3D printed, chemically cross-linked collagen scaffolds (controls) are shown in the Supporting Information (Fig. S7).

To assess the 3D printability of the microparticle-loaded collagen ink toward the generation of clinically relevant shapes, we fabricated meniscus-like structures with the typical C-shape and a wedge-like vertical cross-section, as well as human nose- and auricle-like structures based on generic models (Fig. 6a, b and c). All 3D printed structures preserved high shape fidelity and were stable over time in PBS,

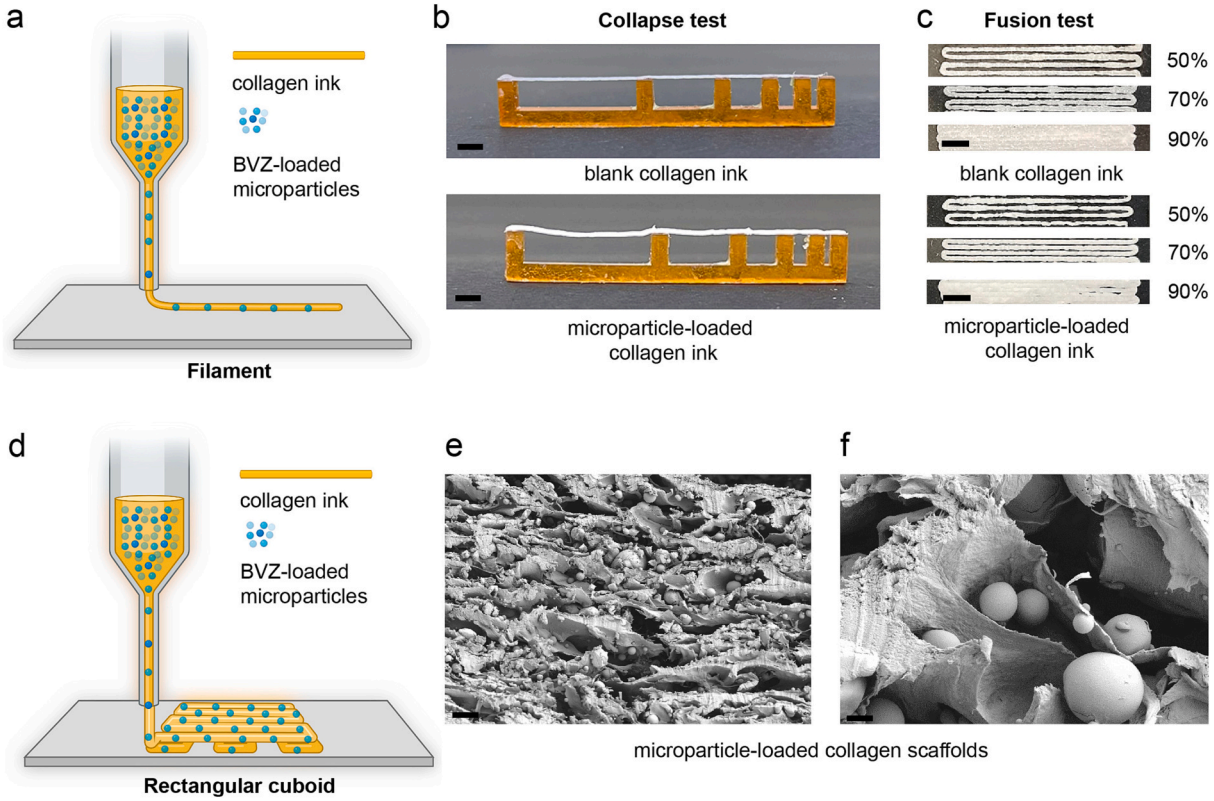

Fig. 5. 3D printing of microparticle-loaded collagen ink and collagen scaffolds. 3D printing of a single filament (a) of the microparticle-loaded collagen ink and blank collagen ink (control) in a filament collapse test (b, scale bar = 4 mm) and a filament fusion test (c, scale bar = 4 mm). Results for the filament fusion test are shown for three different infill values, *i.e.*, 50%, 70% and 90%. 3D printing of multi-layer rectangular cuboids (d) for the fabrication of microparticle-loaded collagen scaffolds. Cross-sections of microparticle-loaded collagen scaffolds after chemical cross-linking and freeze-drying, as visualized by SEM (e, scale bar = 20 μm and f, scale bar = 2 μm).

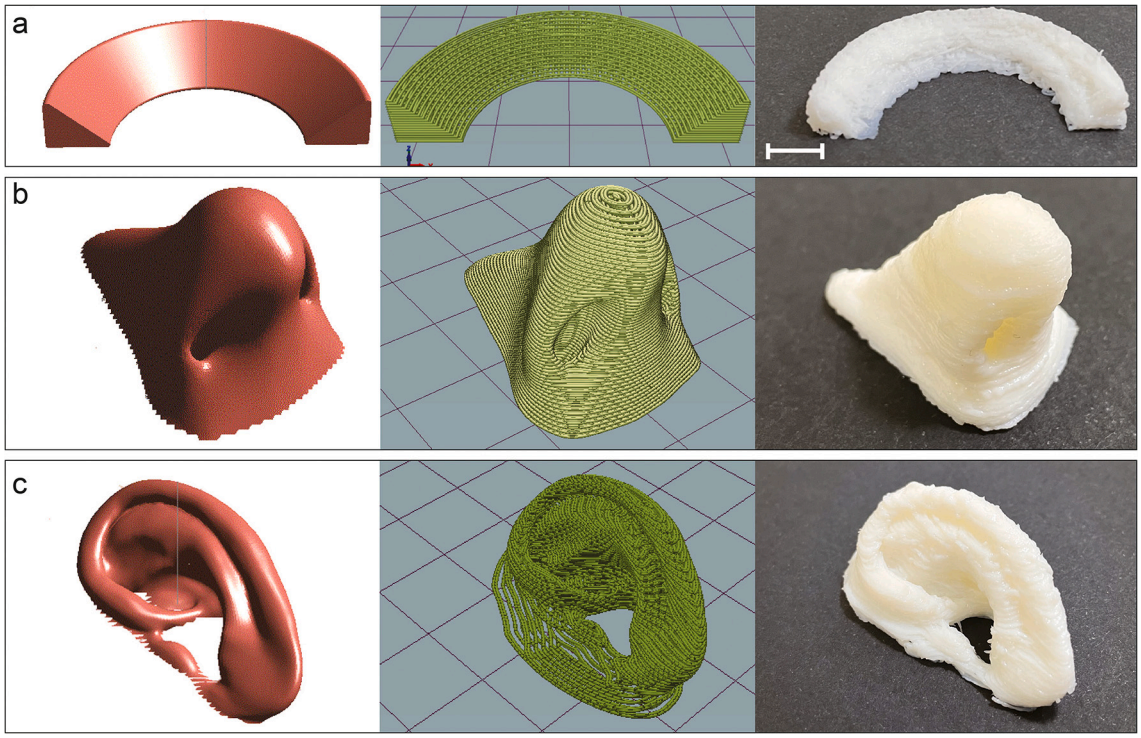

Fig. 6. 3D printing of biomimicking complex structures. Structures resembling the human meniscus (a), nose (b) and auricle (c), obtained by a multi-layer deposition of BVZ microparticle-loaded collagen ink through a "Rokit Invivo 4D2" bioprinter. 3D models based on the STL file (red, left), 3D models showing the printing pattern based on the GCode (green, centre), 3D printed structures (white, right). Scale bar = 1 cm for all 3D printed structures. (For interpretation of the references to colour in this figure legend, the reader is referred to the web version of this article.)

without being chemically cross-linked. Importantly, these structures were 3D printed without a supporting thermoplastic frame or a sacrificial material. The bottom-up fabrication was obtained by the progressive small increments of subsequent layers without intermediate steps of chemical cross-linking. Remarkably, with this procedure both nasal and auricle cavities remained hollow highlighting the printing stability of the microparticle-loaded collagen ink.

The successful 3D printing of these complex structures demonstrated that the applicability of the ink under study could be potentially extended to different tissues for a broad application in tissue engineering. These findings are a valuable effort toward addressing the constant clinical need for personalized medicine in tissue engineering which requires 3D (bio-)printable materials for the fabrication of high-resolution, patient-specific scaffolds. In the last decade, the use of 3D printed collagen inks has been widely reported for tissue engineering application, *e.g.*, for cartilage and bone regeneration [28,56,57]. Usually, collagen is used alone or blended with other materials to obtain synergetic effects on mechanical and biochemical properties. However, most of these studies cover the 3D printing of simple 3D structures, usually rectangular cuboids, or cylinders. Only a few recent papers demonstrated the possibility to print more complex, hollow structures using collagen-based inks, without supporting materials [27,30,58]. It is important to mention that these studies do not include the ink biofunctionalization through drug-loaded delivery systems, *e.g.*, nano- or microparticles which can be a valuable tool for the final *in vivo* performance of the implant. On the other hand, studies that focus on the 3D printing of collagen inks functionalized with nano- and micro-sized drug delivery systems are limited to bone regeneration only and do not consider the possibility of fabricating complex, hollow structures [59–61]. In conclusion, our overview of the data reported in the literature to date confirms the novelty of the work described herein, consisting of a combination of an anti-angiogenic drug delivery system with a medical grade collagen ink for the 3D printing of complex, hollow structures without supporting materials. Future studies will investigate the release kinetics of BVZ from microparticle-loaded collagen scaffolds. In this context, we can hypothesize that the highly porous structure of the collagen scaffold and its interconnected pores are expected to allow the diffusion of the BVZ released from the microparticles *in vitro*. In an *in vivo* setting, when the scaffold is locally implanted, BVZ release kinetics may be affected by additional factors, such as the scaffold infiltration by endogenous components *e.g.*, plasma and cells, and the formation of a fibrin clot. Remarkably, the studied biomaterial is made of FDA-approved and clinically used components, *i.e.*, Avastin® (bevacizumab), medical grade collagen from Geistlich Pharma AG and PLGA. This will potentially accelerate the next steps of investigations toward the clinical translation of the proposed biomaterial.

4. Conclusions

In this study, we achieved the biofunctionalization of a 3D printed, medical grade collagen with BVZ-loaded microparticles to target pathological angiogenesis, as that found in the articular cartilage and meniscus of OA patients. Our findings are of relevance considering the growing interest in the biofunctionalization of tissue engineering constructs by the inclusion of growth factors and other biomolecules. Since these signaling molecules require a molecule-specific spatio-temporal delivery, the combination of 3D printing (spatial control) and drug delivery strategies (temporal control), as explored in this study, is an essential tool for the development of novel tissue constructs with high performance. Likewise, we are currently investigating a similar approach to distribute microparticles loaded with different active factors (pro-angiogenic *vs* anti-angiogenic) throughout meniscus scaffolds to mimic its outer-inner gradient.

CRediT authorship contribution statement

Anna Abbadessa: Conceptualization, Data curation, Investigation, Methodology, Supervision, Validation, Visualization, Writing – original

draft, Writing – review & editing. **Paulina Nuñez Bernal:** Data curation, Formal analysis, Investigation, Methodology, Software, Validation, Visualization, Writing – review & editing. **Giorgio Buttitta:** Investigation, Validation, Writing – review & editing. **Alfredo Ronca:** Data curation, Investigation, Methodology, Software, Validation, Visualization, Writing – review & editing. **Ugo D'Amora:** Data curation, Investigation, Methodology, Software, Validation, Visualization, Writing – review & editing. **Carla Zihlmann:** Investigation, Methodology, Validation, Writing – review & editing. **Niklaus Stiefel:** Funding acquisition, Methodology, Resources, Validation, Writing – review & editing. **Luigi Ambrosio:** Funding acquisition, Resources, Writing – review & editing. **Jos Malda:** Conceptualization, Funding acquisition, Resources, Writing – review & editing. **Riccardo Levato:** Conceptualization, Funding acquisition, Writing – review & editing. **José Crecente-Campo:** Conceptualization, Funding acquisition, Supervision, Writing – review & editing. **María José Alonso:** Conceptualization, Funding acquisition, Project administration, Resources, Supervision, Writing – review & editing.

Declaration of Competing interest

Niklaus Stiefel and Carla Zihlmann are employees of Geistlich Pharma AG. Geistlich Pharma AG provided the collagen material used in this study. Geistlich Pharma AG manufactures and commercializes collagen-based products for tissue regeneration. The other authors do not have any conflict of interests.

Data availability

Data will be made available on request.

Acknowledgements

This project has received funding from the European Union's Horizon 2020 research and innovation program under grant agreement No 814444 (MEFISTO). The authors thank mAbxience-GH Genhelix for the kind donation of Bevacizumab (Avastin®) and Geistlich Pharma AG for providing the medical grade collagen. AA acknowledges funding from "la Caixa" Foundation (ID 100010434) with a fellowship code LCF/BQ/PR22/11920003. RL acknowledges funding from the European Research Council (ERC) under the European Union's Horizon 2020 research and innovation programme (grant agreement No. 949806, VOLUME-BIO). RL and JM acknowledge funding from the Dutch Artritis Foundation (LLP-12 and LLP-22).

Appendix A. Supplementary data

Supplementary data to this article can be found online at https://doi.org/10.1016/j.jconrel.2023.07.017.

References

[1] P. Carmeliet, R.K. Jain, Angiogenesis in cancer and other diseases, Nature 407 (6801) (2000) 249–257.
[2] A. Chopdar, U. Chakravarthy, D. Verma, Age related macular degeneration, Bmj 326 (7387) (2003) 485–488.
[3] P.I. Mapp, D.A. Walsh, Mechanisms and targets of angiogenesis and nerve growth in osteoarthritis, Nat. Rev. Rheumatol. 8 (7) (2012) 390–398.
[4] T. Matsumoto, G.M. Cooper, B. Gharaibeh, L.B. Meszaros, G. Li, A. Usas, F.H. Fu, J. Huard, Cartilage repair in a rat model of osteoarthritis through intraarticular transplantation of muscle-derived stem cells expressing bone morphogenetic protein 4 and soluble Flt-1, Arthritis Rheum. 60 (5) (2009) 1390–1405.
[5] W. Petersen, T. Pufe, C. Stärke, T. Fuchs, S. Kopf, M. Raschke, R. Becker, B. Tillmann, Locally applied angiogenic factors–a new therapeutic tool for meniscal repair, Ann. Anatom. Anatomis. Anzeig. 187 (5–6) (2005) 509–519.
[6] M. Centola, F. Abbruzzese, C. Scotti, A. Barbero, G. Vadala, V. Denaro, I. Martin, M. Trombetta, A. Rainer, A. Marsano, Scaffold-based delivery of a clinically relevant anti-angiogenic drug promotes the formation of in vivo stable cartilage, Tissue Eng. A 19 (17–18) (2013) 1960–1971.
[7] S.M. Kaiser, S. Arepalli, J.P. Ehlers, Current and future anti-VEGF agents for neovascular age-related macular degeneration, J. Exp. Pharmacol. 13 (2021) 905.
[8] T. Bro, M. Derebecka, Ø.K. Jørstad, A. Grzybowski, Off-label use of bevacizumab for wet age-related macular degeneration in Europe, Graefe's Arch. Clin. Exp. Ophthalmol. 258 (3) (2020) 503–511.
[9] S. Lee, J.G.E. Nemeno, J.I. Lee, Repositioning bevacizumab: a promising therapeutic strategy for cartilage regeneration, Tissue Eng. B Rev. 22 (5) (2016) 341–357.
[10] S.K. Chilbule, K. Rajagopal, N. Walter, V. Dutt, V. Madhuri, Role of WNT agonists, BMP and VEGF antagonists in rescuing osteoarthritic knee cartilage in a rat model, Indian J. Orthop. 56 (1) (2022) 24–33.
[11] W. Li, J. Lin, Z. Wang, S. Ren, X. Wu, F. Yu, J. Weng, H. Zeng, Bevacizumab tested for treatment of knee osteoarthritis via inhibition of synovial vascular hyperplasia in rabbits, journal of Orthopaedic, Translation 19 (2019) 38–46.
[12] T. Nagai, M. Sato, T. Kutsuna, M. Kokubo, G. Ebihara, N. Ohta, J. Mochida, Intravenous administration of anti-vascular endothelial growth factor humanized monoclonal antibody bevacizumab improves articular cartilage repair, Arthrit. Res. Therapy 12 (5) (2010) 1–10.
[13] S. Kobsa, W.M. Saltzman, Bioengineering approaches to controlled protein delivery, Pediatr. Res. 63 (5) (2008) 513–519.
[14] F. Li, B. Hurley, Y. Liu, B. Leonard, M. Griffith, Controlled release of bevacizumab through nanospheres for extended treatment of age-related macular degeneration, Open Ophthalmol. J. 6 (2012) 54.
[15] J. Liu, X. Zhang, G. Li, F. Xu, S. Li, L. Teng, Y. Li, F. Sun, Anti-angiogenic activity of bevacizumab-bearing dexamethasone-loaded PLGA nanoparticles for potential intravitreal applications, Int. J. Nanomedicine 14 (2019) 8819.
[16] C.K. Pan, C. Durairaj, U.B. Kompella, O. Agwu, S.C. Oliver, H. Quiroz-Mercado, N. Mandava, J.L. Olson, Comparison of long-acting bevacizumab formulations in the treatment of choroidal neovascularization in a rat model, J. Ocular Pharmacol. Ther. 27 (3) (2011) 219–224.
[17] J. Pandit, Y. Sultana, M. Aqil, Chitosan-coated PLGA nanoparticles of bevacizumab as novel drug delivery to target retina: optimization, characterization, and in vitro toxicity evaluation, Artific. Cells Nanomed. Biotechnol. 45 (7) (2017) 1397–1407.
[18] R. Varshochian, M. Jeddi-Tehrani, A.R. Mahmoudi, M.R. Khoshayand, F. Atyabi, A. Sabzevari, M.R. Esfahani, R. Dinarvand, The protective effect of albumin on bevacizumab activity and stability in PLGA nanoparticles intended for retinal and choroidal neovascularization treatments, Eur. J. Pharm. Sci. 50 (3–4) (2013) 341–352.
[19] F. Sousa, A. Cruz, P. Fonte, I.M. Pinto, M.T. Neves-Petersen, B. Sarmento, A new paradigm for antiangiogenic therapy through controlled release of bevacizumab from PLGA nanoparticles, Sci. Rep. 7 (1) (2017) 1–13.
[20] X.-P. Zhang, J.-G. Sun, J. Yao, K. Shan, B.-H. Liu, M.-D. Yao, H.-M. Ge, Q. Jiang, C. Zhao, B. Yan, Effect of nanoencapsulation using poly (lactide-co-glycolide) (PLGA) on anti-angiogenic activity of bevacizumab for ocular angiogenesis therapy, Biomed. Pharmacother. 107 (2018) 1056–1063.
[21] S. Mohammadi-Samani, B. Taghipour, PLGA micro and nanoparticles in delivery of peptides and proteins; problems and approaches, Pharm. Dev. Technol. 20 (4) (2015) 385–393.
[22] D.G. Armstrong, D.P. Orgill, R.D. Galiano, P.M. Glat, J.P. Kaufman, M.J. Carter, L. A. DiDomenico, C.M. Zelen, Use of a purified reconstituted bilayer matrix in the management of chronic diabetic foot ulcers improves patient outcomes vs standard of care: results of a prospective randomised controlled multi-Centre clinical trial, Int. Wound J. (2022) 1–13.
[23] F.G. Usuelli, L. de Girolamo, M. Grassi, R. D'Ambrosi, U.A. Montrasio, M. Boga, All-arthroscopic autologous matrix-induced chondrogenesis for the treatment of osteochondral lesions of the talus, Arthrosc. Tech. 4 (3) (2015) e255–e259.
[24] F. Schwarz, A. Hegewald, N. Sahm, J. Becker, Long-term follow-up of simultaneous guided bone regeneration using native and cross-linked collagen membranes over 6 years, Clin. Oral Implants Res. 25 (9) (2014) 1010–1015.
[25] J. Becker, B. Al-Nawas, M.O. Klein, H. Schliephake, H. Terheyden, F. Schwarz, Use of a new cross-linked collagen membrane for the treatment of dehiscence-type defects at titanium implants: a prospective, randomized-controlled double-blinded clinical multicenter study, Clin. Oral Implants Res. 20 (7) (2009) 742–749.
[26] A. Schlegel, H. Möhler, F. Busch, A. Mehl, Preclinical and clinical studies of a collagen membrane (Bio-Gide®), Biomaterials 18 (7) (1997) 535–538.
[27] Y. Zhang, S.T. Ellison, S. Duraivel, C.D. Morley, C.R. Taylor, T.E. Angelini, 3D printed collagen structures at low concentrations supported by jammed microgels, Bioprinting 21 (2021), e00121.
[28] X. Yang, Z. Lu, H. Wu, W. Li, L. Zheng, J. Zhao, Collagen-alginate as bioink for three-dimensional (3D) cell printing based cartilage tissue engineering, Mater. Sci. Eng. C 83 (2018) 195–201.
[29] E.V. Isaeva, E.E. Beketov, G.A. Demyashkin, N.D. Yakovleva, N.V. Arguchinskaya, A.A. Kisel, T.S. Lagoda, E.P. Malakhov, A.N. Smirnova, V.M. Petriev, Cartilage formation in vivo using high concentration collagen-based bioink with MSC and decellularized ECM granules, Int. J. Mol. Sci. 23 (5) (2022) 2703.
[30] S. Rhee, J.L. Puetzer, B.N. Mason, C.A. Reinhart-King, L.J. Bonassar, 3D bioprinting of spatially heterogeneous collagen constructs for cartilage tissue engineering, ACS Biomater. Sci. Eng. 2 (10) (2016) 1800–1805.
[31] Y. Koo, E.-J. Choi, J. Lee, H.-J. Kim, G. Kim, S.H. Do, 3D printed cell-laden collagen and hybrid scaffolds for in vivo articular cartilage tissue regeneration, J. Ind. Eng. Chem. 66 (2018) 343–355.
[32] C.-F. Lee, Y.-H. Hsu, Y.-C. Lin, T.-T. Nguyen, H.-W. Chen, S.C. Nabilla, S.-Y. Hou, F.-C. Chang, R.-J. Chung, 3D printing of collagen/oligomeric proanthocyanidin/oxidized hyaluronic acid composite scaffolds for articular cartilage repair, Polymers 13 (18) (2021) 3123.

[33] O. Messaoudi, C. Henrionnet, K. Bourge, D. Loeuille, P. Gillet, A. Pinzano, Stem cells and extrusion 3D printing for hyaline cartilage engineering, Cells 10 (1) (2020) 2.
[34] A. Abbadessa, J. Crecente-Campo, M.J. Alonso, Engineering anisotropic meniscus: zonal functionality and spatiotemporal drug delivery, Tissue Eng. B Rev. 27 (2) (2021) 133–154.
[35] T. Karimi, D. Barati, O. Karaman, S. Moeinzadeh, E. Jabbari, A developmentally inspired combined mechanical and biochemical signaling approach on zonal lineage commitment of mesenchymal stem cells in articular cartilage regeneration, Integr. Biol. 7 (1) (2014) 112–127.
[36] D. Blanco, M.J. Alonso, Protein encapsulation and release from poly (lactide-co-glycolide) microspheres: effect of the protein and polymer properties and of the co-encapsulation of surfactants, Eur. J. Pharm. Biopharm. 45 (3) (1998) 285–294.
[37] I. Pennings, L.A. van Dijk, J. van Huuksloot, J.O. Fledderus, K. Schepers, A. K. Braat, E.C. Hsiao, E. Barruet, B.M. Morales, M.C. Verhaar, A.J.W.P. Rosenberg, D. Gawlitta, Effect of donor variation on osteogenesis and vasculogenesis in hydrogel cocultures, J. Tissue Eng. Regen. Med. 13 (3) (2019) 433–445.
[38] E. Zudaire, L. Gambardella, C. Kurcz, S. Vermeren, A computational tool for quantitative analysis of vascular networks, PLoS One 6 (11) (2011), e27385.
[39] A. Ribeiro, M.M. Blokzijl, R. Levato, C.W. Visser, M. Castilho, W.E. Hennink, T. Vermonden, J. Malda, Assessing bioink shape fidelity to aid material development in 3D bioprinting, Biofabrication 10 (1) (2017), 014102.
[40] R. Dinarvand, S. Moghadam, A. Sheikhi, F. Atyabi, Effect of surfactant HLB and different formulation variables on the properties of poly-D, L-lactide microspheres of naltrexone prepared by double emulsion technique, J. Microencapsul. 22 (2) (2005) 139–151.
[41] M.C. Benéitez, J.I. Espada, D. Fernandes, D.H.P. de la Ossa, M.E. Gil-Alegre, Influence of surfactant on the characteristics of W1/O/W2-microparticles, J. Surfactant Deterg. 17 (1) (2014) 11–18.
[42] R. Varshochian, M. Riazi-Esfahani, M. Jeddi-Tehrani, A.R. Mahmoudi, S. Aghazadeh, M. Mahbod, M. Movassat, F. Atyabi, A. Sabzevari, R. Dinarvand, Albuminated PLGA nanoparticles containing bevacizumab intended for ocular neovascularization treatment, J. Biomed. Mater. Res. A 103 (10) (2015) 3148–3156.
[43] F. Sousa, A. Cruz, I.M. Pinto, B. Sarmento, Nanoparticles provide long-term stability of bevacizumab preserving its antiangiogenic activity, Acta Biomater. 78 (2018) 285–295.
[44] J. Panyam, M.M. Dali, S.K. Sahoo, W. Ma, S.S. Chakravarthi, G.L. Amidon, R. J. Levy, V. Labhasetwar, Polymer degradation and in vitro release of a model protein from poly (D, L-lactide-co-glycolide) nano-and microparticles, J. Control. Release 92 (1–2) (2003) 173–187.
[45] N. Samadi, A. Abbadessa, A. Di Stefano, C. Van Nostrum, T. Vermonden, S. Rahimian, E. Teunissen, M. Van Steenbergen, M. Amidi, W. Hennink, The effect of lauryl capping group on protein release and degradation of poly (d, l-lactic-co-glycolic acid) particles, J. Control. Release 172 (2) (2013) 436–443.
[46] G. Crotts, T.G. Park, Protein delivery from poly (lactic-co-glycolic acid) biodegradable microspheres: release kinetics and stability issues, J. Microencapsul. 15 (6) (1998) 699–713.
[47] T.G. Park, W. Lu, G. Crotts, Importance of in vitro experimental conditions on protein release kinetics, stability and polymer degradation in protein encapsulated poly (D, L-lactic acid-co-glycolic acid) microspheres, J. Control. Release 33 (2) (1995) 211–222.
[48] S. Narayana, M.G. Ahmed, A. Nasrine, Effect of nano-encapsulation using human serum albumin on anti-angiogenesis activity of bevacizumab to target corneal neovascularization: development, optimization and in vitro assessment, Mater. Today Proc. 68 (2022) 93–104.
[49] E. Peira, G. Chindamo, D. Chirio, S. Sapino, S. Oliaro-Bosso, E. Rebba, P. Ivanchenko, M. Gallarate, Assessment of in-situ gelling microemulsion systems upon temperature and dilution condition for corneal delivery of bevacizumab, Pharmaceutics 13 (2) (2021) 258.
[50] K. Park, A. Otte, F. Sharifi, J. Garner, S. Skidmore, H. Park, Y.K. Jhon, B. Qin, Y. Wang, Formulation composition, manufacturing process, and characterization of poly (lactide-co-glycolide) microparticles, J. Control. Release 329 (2021) 1150–1161.
[51] P.N. Bernal, M. Bouwmeester, J. Madrid-Wolff, M. Falandt, S. Florczak, N. G. Rodriguez, Y. Li, G. Größbacher, R.A. Samsom, M. van Wolferen, L. van der Laan, P. Delrot, D. Loterie, J. Malda, C. Moser, B. Spee, R. Levato, Volumetric bioprinting of organoids and optically tuned hydrogels to build liver-like metabolic biofactories, Adv. Mater. 34 (15) (2022) 2110054.
[52] M.L. Terpstra, J. Li, A. Mensinga, M. de Ruijter, M.H. van Rijen, C. Androulidakis, C. Galiotis, I. Papantoniou, M. Matsusaki, J. Malda, R. Levato, Bioink with cartilage-derived extracellular matrix microfibers enables spatial control of vascular capillary formation in bioprinted constructs, Biofabrication 14 (3) (2022), 034104.
[53] L. García-Fernández, S. Halstenberg, R.E. Unger, M.R. Aguilar, C.J. Kirkpatrick, J. San Román, Anti-angiogenic activity of heparin-like polysulfonated polymeric drugs in 3D human cell culture, Biomaterials 31 (31) (2010) 7863–7872.
[54] K.T. Morin, R.T. Tranquillo, In vitro models of angiogenesis and vasculogenesis in fibrin gel, Exp. Cell Res. 319 (16) (2013) 2409–2417.
[55] L. Bédouet, V. Verret, S. Louguet, E. Servais, F. Pascale, A. Beilvert, M.-T. Baylatry, D. Labarre, L. Moine, A. Laurent, Anti-angiogenic drug delivery from hydrophilic resorbable embolization microspheres: an in vitro study with sunitinib and bevacizumab, Int. J. Pharm. 484 (1–2) (2015) 218–227.
[56] H. Suo, J. Zhang, M. Xu, L. Wang, Low-temperature 3D printing of collagen and chitosan composite for tissue engineering, Mater. Sci. Eng. C 123 (2021), 111963.
[57] H. Lee, G.H. Yang, M. Kim, J. Lee, J. Huh, G. Kim, Fabrication of micro/nanoporous collagen/dECM/silk-fibroin biocomposite scaffolds using a low temperature 3D printing process for bone tissue regeneration, Mater. Sci. Eng. C 84 (2018) 140–147.
[58] C.C. Clark, J. Aleman, L. Mutkus, A. Skardal, A mechanically robust thixotropic collagen and hyaluronic acid bioink supplemented with gelatin nanoparticles, Bioprinting 16 (2019), e00058.
[59] F. Banche-Niclot, C. Licini, G. Montalbano, S. Fiorilli, M. Mattioli-Belmonte, C. Vitale-Brovarone, 3D printed scaffold based on type I collagen/PLGA_TGF-β1 nanoparticles mimicking the growth factor footprint of human bone tissue, Polymers 14 (5) (2022) 857.
[60] G. Montalbano, G. Borciani, G. Cerqueni, C. Licini, F. Banche-Niclot, D. Janner, S. Sola, S. Fiorilli, M. Mattioli-Belmonte, G. Ciapetti, Collagen hybrid formulations for the 3d printing of nanostructured bone scaffolds: an optimized genipin-crosslinking strategy, Nanomaterials 10 (9) (2020) 1681.
[61] F. Banche-Niclot, G. Montalbano, S. Fiorilli, C. Vitale-Brovarone, PEG-coated large mesoporous silicas as smart platform for protein delivery and their use in a collagen-based formulation for 3D printing, Int. J. Mol. Sci. 22 (4) (2021) 1718.